

O₂ adsorption on Au_nRh n = 1–5 neutral and charged clusters

Fernando Buendía and Marcela R. Beltrán^a

Instituto de Investigaciones en Materiales, Universidad Nacional Autónoma de México Circ. ext. s/n Apdo.
Postal 70-360, C.P. 04510, México D.F., México

Received 23 October 2015 / Received in final form 27 January 2016

Published online 5 April 2016 – © EDP Sciences, Società Italiana di Fisica, Springer-Verlag 2016

Abstract. Theoretical evidence is presented for the molecular and dissociative adsorption of O₂ on free Au_nRh neutral, anionic and cationic clusters with 1 to 5 gold atoms, indicating that the stabilization of the activated di-oxygen species is a key factor for the unusual catalytic activities of Au-based catalysts. The structure, stability, for both molecular and dissociative O₂ adsorption on Au_nRh n = 1–5 clusters has been investigated using density-functional theory. To find the transition states, the minimum energy paths have been explored for a few clusters. In general, lower values for the activation energy have been found when compared with the barriers that occur on pure Au_n based clusters. The higher binding energies in the AuRh mix favor oxygen dissociation among any other possible reaction paths. The anionic clusters being the most reactive of all. The molecular bonding mechanism to these complexes involves charge transfer to the oxygen molecule with a concomitant activation of the O–O bond to a superoxo-like state. The characteristic planar structures of both pure gold and AuRh clusters prevail for most of the cases here studied. The odd-even characteristic catalytic activation of pure gold clusters is not observed once even a single rhodium atom has been added to the cluster.

1 Introduction

Small clusters and nanoparticles are of great interest from both, fundamental and technological points of view. One important aspect of them is their potential applications towards catalysis. Haruta found that dispersed gold nanoparticles show catalytic activity toward the oxidation of CO [1–4]. This fact has triggered a gold rush in the cluster chemistry community over the last years, where a number of studies [5–10], have found that gold at the nanoscale presents catalytic reactivity towards a number of substances like O₂, CO, NO_x, etc., and this behavior is size-dependent in both, gas phase and deposited clusters. Negatively charged clusters with an even number of atoms (odd number of valence electrons) show significant O₂ uptake, whereas odd-numbered clusters either are not prone to react with oxygen, or show very weak reactivity [10–24]. It is believed that small particles of gold differ from the bulk because they contain edge atoms that have low coordination and can adopt different geometries leading to more reactive sites. Thus, the catalytic properties of gold nanoparticles lies partly in their geometric structure [6]. On the other hand bimetallic nanoparticles often referred to as nanoalloys have been proposed in recent years [25–28]. One of the reasons for the increasing interest is that their properties can be tuned even further by varying not only the size as in pure monometallic clusters, but also their composition [29]. This is pre-

cisely the subject of this work, we will study how their reactivity is substantially modified not only by changing their size and their structure but also, their charge state and their chemical composition when rhodium is added. Rhodium has been known as an heterogeneous catalytic material for many years [30–32], and at the nanoscale it has proved to be one of the best components for the removal of NO_x, a very important step in pollution-control processes [33–36]. As the starting point for our study of free nanoalloy clusters is the determination of their most favorable structures. Therefore, a systematic theoretical and experimental study of the stability of Au–Rh bimetallic clusters has been previously performed and published by us, where the global minima and the electronic and magnetic properties of Au_nRh_m n = 1–6, m = 1, 2 clusters have been determined [37]. In the present work we want to shed light on the adsorption properties of oxygen on AuRh clusters simulating their behavior under oxygen rich simulated atmosphere. The methodology used to perform this study is the density functional theory (DFT). We consider the adsorption of O₂ on Au_nRh n = 1–5 neutral as well as positively and negatively charged clusters. We have searched the lowest local minima exploring a wide range of reasonable geometric configurations in a separate manner for both, molecular O₂ adsorption (MA) as well as dissociative O₂ adsorption (DA) on to the previously converged Au_nRh_m structures obtained in reference [37]. The spin manifold has been equally explored for neutral as well as charged clusters and for both: MA and DA states. Furthermore, the transition state from the

^a e-mail: mbeltran@unam.mx

Table 1. Comparison between the available experimental data with this work.

| Dimmer | ω (cm^{-1}) | E_b (eV) | R_{eq} \AA |
|-------------------|----------------------------------|---------------|--------------------------|
| Au-Au | 171 | 2.23 | 2.53 |
| Exp. ^a | 190 | 2.29 | 2.47 |
| Au-Rh | 196 | 2.41 | 2.50 |
| Rh-Rh | 289 | 3.17 | 2.32 |
| Exp. ^b | 267 | — | 2.28 |
| O-O | 1555 | 6.25 | 1.22 |
| Exp. ^c | 1580 | 5.11 | 1.21 |

^a Previous experimental values see reference [44]. ^b Previous experimental values see reference [45]. ^c Previous experimental values see reference [46].

molecular towards the dissociative state has been analysed carefully in each case by means of a nudge bond model method developed by us and which will be described here. We will be presenting and discussing: the electron affinity (EA), ionization potential (IP), binding energies (E_b), spin multiplicities, gaps, infrared (IR) spectra and fragmentation energies (ΔE) for molecular (MA) and dissociative (DA) O₂ clusters. Their dissociation energies for different evaporation channels have also been calculated, and finally the influence of the adsorption on the structure, and the stability of the clusters is also discussed. Our conclusions are given in the final section.

2 Computational details

The density functional theory (DFT) approximation has been used in the present study. The calculation of the Coulomb integrals has been made by means of the RI-J method to reduce the computing time. The def2-TZVP basis set has been employed (with the associated effective core potential def2-ecp which considers 19 explicit valence electrons for gold and 17 for rhodium) [38] and includes relativistic effects. The Perdew, Becke and Erzenhoff [39] exchange and correlation functional has been chosen as it has proven to be highly efficient and precise in the study of gold clusters [40,41]. The convergence parameter for the energy in the self-consistent field is 10^{-6} Ha. The calculations have been performed following a steep descent until forces dropped below a threshold value of 1×10^{-3} Ha/Bohr and the Hartree energy is converged to 10^{-6} Ha at each cycle. The calculation has been performed under the internal coordinates framework. The geometry optimizations were carried out without imposing any symmetry constraints, to allow full variational freedom. This study has been made by means of the TURBOMOLE V6.4 package [42]. In order to calibrate our methodology, first of all we compare some of our results with previous theoretical calculations [43] and with the available experimental data [44–46], such comparison can be seen in Table 1 for Au₂, Rh₂, O₂ and AuRh. In the case of pure gold, we have found a bond length of 2.53 Å, that compares well with the 2.47 Å experimental value [44]. For rhodium we

obtain 2.29 Å which is very similar to the experimental value of 2.28 Å [45]. For the AuRh mix we have calculated a bond length of 2.41 Å, and a vibrational frequency of 196 cm^{-1} for which no previous experimental data is available. Our result agrees well with the previously calculated value of 2.52 Å for the bond length and the frequency of 199 cm^{-1} in reference [43]. Finally for O₂ we obtained an equilibrium O-O distance of 1.22 Å, which compares well with 1.21 Å from the experiment [46]. The calculated bond lengths have been used as a parameter as initial guess in the symmetry unrestricted and unconstrained search for the lowest minima structures here presented. These values are benchmarks to guarantee the effectivity of the whole theoretical framework. Furthermore we compared our calculated infrared spectra (IR) for pure gold clusters with experimental Far infrared multiphoton dissociation (FIR-MPD) data from reference [10], and we obtain a very good agreement. The harmonic vibrational frequencies have been calculated first to verify true low energy landscape minimum states and to be compared directly with possible future experimental data from Far infrared (FIR-MPD) spectra on the same systems. Our infrared spectra are produced with a Gaussian function of FWHM 25 cm^{-1} . They were performed for all lowest minima and for charged as well as for neutral Au_nRhO₂ clusters (for $n = 1-5$). We explored all inequivalent positions for the Au and Rh atoms as well. Low energy structures of Au_nRh have been fully investigated and reported in an earlier publication [37]. In this work O₂ are added to the bare Au_nRh $n = 1-5$. Hollow, top and bridge positions have been investigated for all possible surface sites. First, an O₂ molecule has been adsorbed and secondly dissociated O atoms have been adsorbed onto the clusters surfaces. Therefore the two possible states with the oxygen molecularly adsorbed (MA) and dissociatively adsorbed (DA) have been searched for separately. The total magnetic moments have been calculated from the Mulliken populations, from the majority and minority spin configurations. The cluster energies in this work are the sum of the electronic and vibrational contributions calculated from the zero point vibrational energies.

The transition state between the molecular ground state to the dissociative ground state has been explored by means of a locally developed methodology. Our methodology is based on the drag method or the reaction coordinate, which belongs to a family of the so called nudge elastic band methods [47]. Where some subset of the coordinates in the system is used to define the progress variable (in our case the O-O distance), through a linear interpolation between the initial to the final configurations. This one degree of freedom is then varied stepwise from the initial to the final value and at each step a minimization is carried out over the remaining degrees of freedom (a total of $(3N - 1)$ degrees of freedom if the system consists of N atoms in 3 dimensions). While this method can work well in simple cases, there are many instances where it fails. The path generated may be discontinuous and the procedure may depend on the direction of the drag (hysteresis effects). In particular some atomic coordinates may slip

near the saddle point region and the saddle point configurations will then be missed. This has been avoided by verifying the saddle point or transition state by checking that it possess one and only one imaginary frequency.

3 Results and discussion

In this section we present results for oxygen adsorption on the surfaces of neutral, anionic and cationic Au_nRhO_2 ($n = 1-5$) clusters. We have proceed as follows: for each cluster size, the global minima for both, molecular and dissociative adsorption of two oxygen atoms have been calculated independently. A deep search in the potential energy surface (PES) minima has been performed without any symmetry constraints including the exploration of the spin manifold. The minima have been verified by means of the frequency analysis. Following this, we have proceeded to explore the transition state between the molecular (MA) and the dissociative (DA) states by means of a drag type methodology, also known as 'reaction coordinate method' which has been discussed in the previous section.

Au_nRhO_2

The geometries for the Au_nRhO_2 $n = 1-5$ neutral lowest energy structures where the oxygen is molecularly adsorbed (MA) clusters are shown in Figure 1. Those structures are actually very similar to the geometries obtained in an earlier work, where Au_nRh pure clusters are studied [37]. The first important result to remark is that the rhodium atom acts always as the preferred adsorption site for the oxygen molecule. Another interesting result is that these clusters are planar except for the oxygen atoms which are off the plane formed by AuRh core in Au_4RhO_2 and Au_5RhO_2 .

We show the lowest minima geometries for neutral Au_nRhO_2 $n = 1-5$ clusters where the oxygen is dissociatively adsorbed (DA) in the lower part of Figure 1. We find that the geometries would be planar and just as the ones found in our previous Au_nRh_m study [37], with the exception of the oxygen atoms, which are located off the plane formed by the cluster, rendering to the whole structure a three dimensional nature. With the exemption of Au_5RhO_2 for which a complete conformational structural change is observed, due to the formation of new chemical bonds between the gold atoms and the dissociated oxygen molecule. It has also been observed that as we increase the number of gold atoms, the oxygen binding energy ($E_b(\text{O}_2)$) for both DA and MA states decreases. This behavior starts to mimic in certain way the adsorption of O_2 in a pure gold cluster scenario [14,16]. This is evidenced in the oxygen binding energies shown in Table 2, where the cluster multiplicities, the HOMO-LUMO's, the O_2 Binding energies, the charge transfer and the activation energies are shown. In general we have observed that the dissociative state is more stable than the molecular one. This follows from the analysis of the di-oxygen binding energies $E_b(\text{O}_2)$ for the DA clusters, which are always bigger than the $E_b(\text{O}_2)$ of the MA clusters (Tab. 2

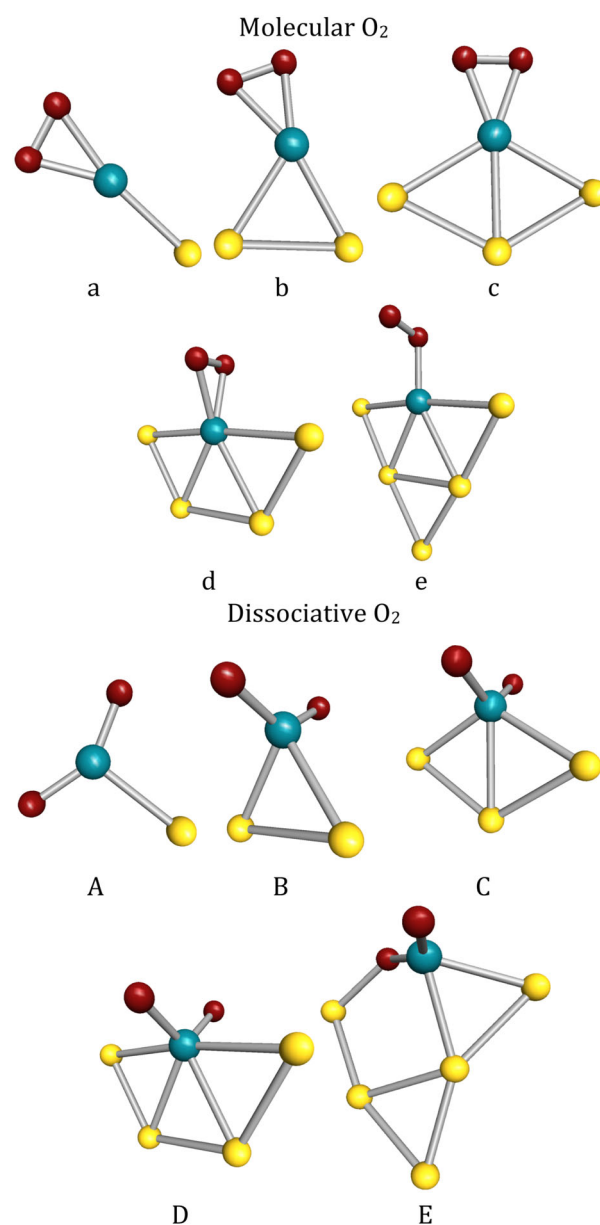


Fig. 1. Structures for atomic Au_nRhO_2 $n = 1-7$ neutral clusters with molecularly O_2 and dissociatively O_2 adsorbed onto their surfaces.

columns 6 and 7). They have been calculated following the next expression:

$$E_b(\text{O}_2) = E(\text{Au}_n\text{RhO}_2) - [E(\text{Au}_n\text{Rh}) + E(\text{O}_2)].$$

The next step was to study the behavior of the reaction path exploring the potential energy surface for each cluster. This has been performed by sampling around 400 points between the molecular and the dissociative adsorption state and its spin manifold at each cluster size by means of the methodology explained in the computational details section. We present in Table 2 the activation energy barriers from our calculations for the neutral cluster cases. And it is defined as the difference between the energy of the MA state and the energy of the transition state

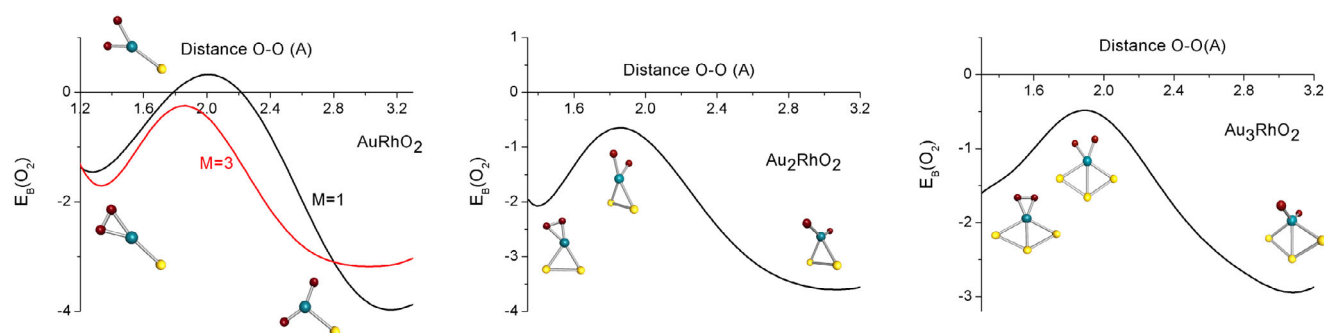


Fig. 2. Calculated reaction energy paths for the O_2 dissociation for Au_nRhO_2 , $n = 1-3$ neutral clusters.

Table 2. Spin multiplicities, HOMO-LUMO gap's, oxygen binding energies, charge transfer from the cluster to the oxygen atoms and activation energies for both, MA and DA states for Au_nRhO_2 , $n = 1-5$ neutral clusters.

| Cluster | 2S+1 | | GAP(H-L) | | $E_b(O_2)$ | | ΔQ (e^-) | E_{act} (eV) |
|-------------|------|----|----------|------|------------|------|-------------------------|-------------------|
| | MA | DA | MA | DA | MA | DA | | |
| | | | | | | | | |
| $AuRhO_2$ | 3 | 1 | 0.47 | 1.39 | 1.54 | 3.78 | 0.64 | 1.62 |
| Au_2RhO_2 | 2 | 2 | 0.38 | 0.45 | 1.94 | 3.45 | 0.66 | 1.64 |
| Au_3RhO_2 | 3 | 3 | 0.40 | 0.60 | 1.57 | 2.74 | 0.72 | 1.16 |
| Au_4RhO_2 | 2 | 2 | 0.46 | 0.28 | 1.54 | 2.26 | 0.70 | 1.35 |
| Au_5RhO_2 | 3 | 1 | 0.37 | 0.78 | 0.92 | 2.19 | 0.66 | 1.62 |

(TS) in the minimum energy path (MEP):

$$E_{act}(Au_nRhO_2) = E(Au_nRhO_2)_{MA} - E(Au_nRhO_2)_{TS}.$$

Their values range from 1.16 eV to 1.64 eV. The first result to be noticed is that the values we obtained are approximately half of those typically found on pure gold clusters with the same number of atoms, see for those obtained by Häkkinen and Landman in reference [14]. The following discussion will be based on the behavior of the multiplicity along the MEP. We categorize them in three possible scenarios:

- $AuRhO_2$ and Au_5RhO_2 , for these two systems the multiplicity changes as we move along the MA and the DA state along the reaction path. The dissociation of the O_2 brings a decrease in the spin multiplicity linked with an increase of the HOMO-LUMO gap (see Tab. 2). The rearrangement in the spin manifold occurs well after the O_2 dissociation has already taken place as can be seen in a representative figure of the minimum energy path (MEP) for the $AuRhO_2$ case, in Figure 2a. Their relatively low activation energies (1.62 eV) make them good candidates for catalysis.
- Au_2RhO_2 and Au_4RhO_2 have the lowest possible spin multiplicity ($M = 2$) along their trajectories, possessing also a relatively low activation energy of 1.64 and 1.35 eV respectively as can be seen in Table 2. The MEP is graphically shown for Au_2RhO_2 in Figure 2b.

- Au_3RhO_2 is unique in the sense that this is the only system with 2 unpaired electrons, and despite that it maintains its multiplicity after the dissociation of O_2 . An important result is that this system has the smallest activation energy (1.16 eV) of all the neutral clusters here studied see Table 2 and its MEP in Figure 2c.

The electronic charge has been calculated by means of the Mulliken approximation and it is also reported in Table 2. We found a charge transfer towards the oxygen atoms from the rhodium atom as it was expected. This promotes a superoxo-like state with the dissociation of the oxygen molecule.

Following this, we produced the Au_nRhO_2 $n = 1-5$ infrared spectra for both MA and DA states, they are shown in Figure 3.

The most representative peaks are in the high frequency region ($500-1500\text{ cm}^{-1}$) and are related with the oxygen vibrations. For the MA states, the one associated with the characteristic O-O stretching is located at around 1000 to 1200 cm^{-1} , depending on the system and is the most intense (graphs on the left column in Fig. 3). This value is different compared with the molecular O_2 vibrational mode (1555 cm^{-1}) in the gas phase. This is due to the fact that the O-O bond is being weakened by the clusters. The O-O breaking in the dissociative systems (DA) lowers even further both, the frequency ($200-300\text{ cm}^{-1}$) and the intensity. Therefore the most representative peaks are the symmetrical and the antisymmetrical stretching modes associated with the strengthened Rh-O bonds, and they are located around 700 and 900 cm^{-1} (shown in the right column in Fig. 3).

Summarizing the results for the neutral clusters we can conclude that the stability for the dissociative states is favored over the molecular states in all cases. Furthermore, the activation energy for the dissociation of O_2 in the cases of Au_nRhO_2 for $n = 2-4$ is smaller than the oxygen binding energy of Au and O_2 separately. This allows the dissociation of oxygen as the most probable pathway for reaction. If we compare the activation energies of the well studied gold atoms for the same atomic sizes [6,7,14,16,20], we found that AuRh mix is a much better candidate to weaken the O-O bond.

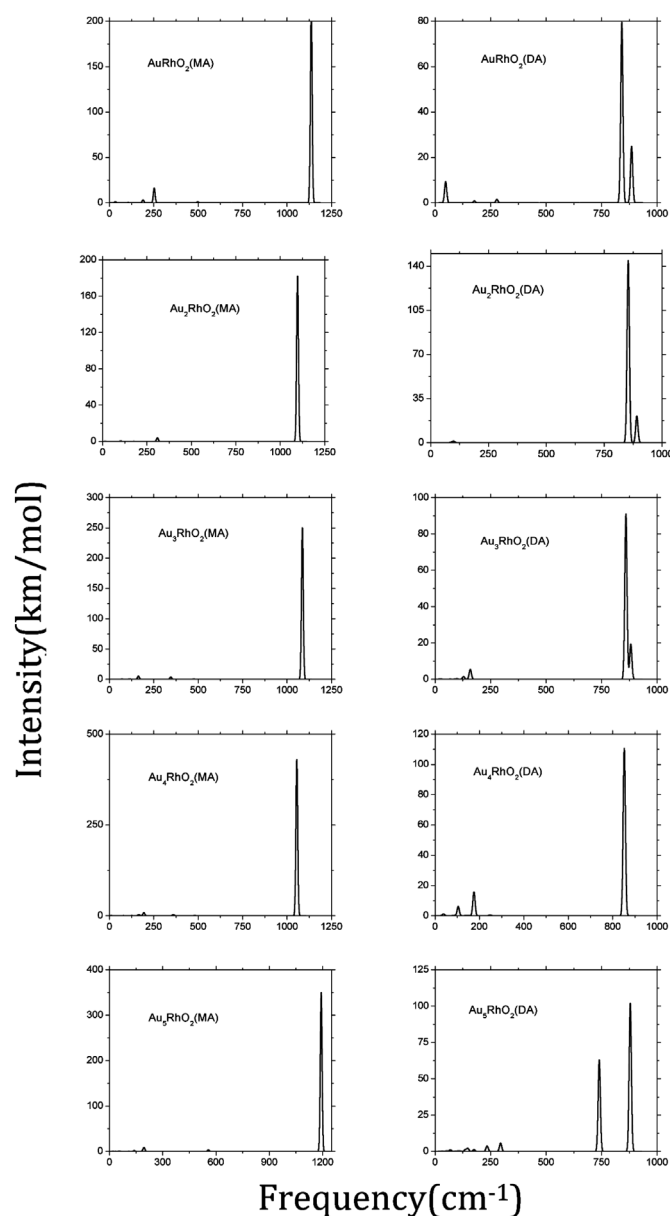


Fig. 3. Infra red calculated spectra for both molecularly bound O_2 (left) and dissociatively bound O_2 (right) for Au_nRhO_2 , $n = 1-5$ neutral clusters.

$Au_nRhO_2^-$

The ground state geometries for the anionic $Au_nRhO_2^-$ MA systems are planar and very similar to the Au_nRh^- clusters reported in reference [37], with the exemption of the O_2 molecule which is perpendicular to the plane formed by the Au_nRh cluster, this can be seen in the series of figures in upper most part in Figure 4. Notice how the preferred binding site for the oxygen molecule is the rhodium atom. The binding energies with the O_2 molecule are relatively bigger with respect to the neutrals, and are reported in Table 3.

For the DA state the oxygen atoms are again located out of the plane like in the MA systems (see the series of figures in lowest part in Fig. 4), and even more, their

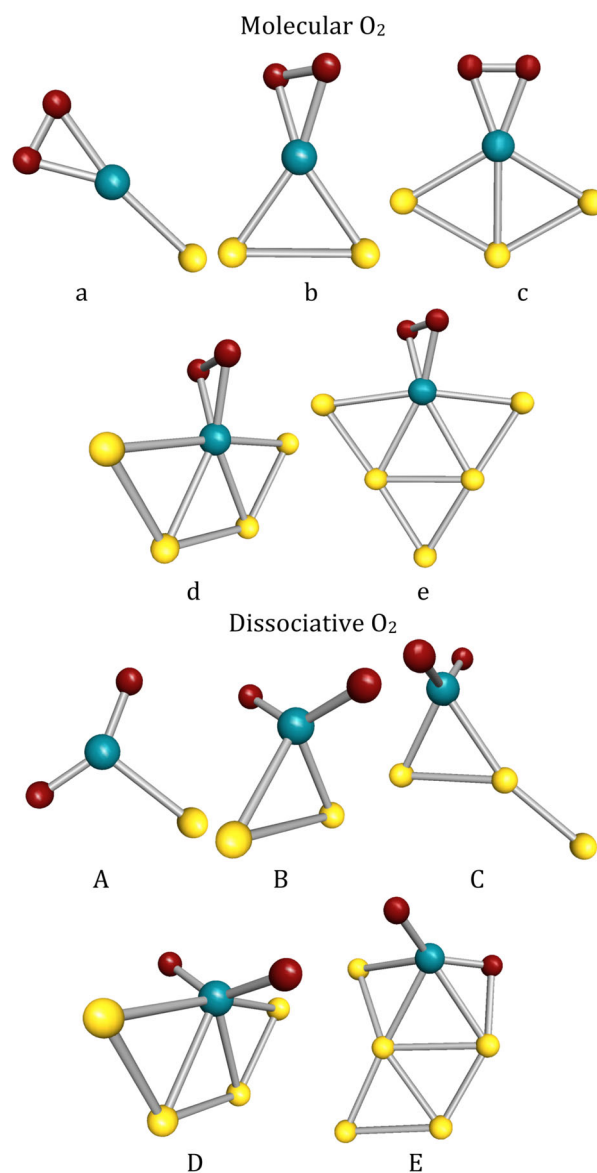


Fig. 4. Structures for atomic $Au_nRhO_2^-$ $n = 1-7$ anionic clusters with molecularly and dissociatively O_2 adsorbed O_2 onto their surfaces.

binding energies increase with respect to the MA clusters, favoring the dissociative state over the molecular one (see Tab. 3). When comparing the results from Tables 2 and 3 we can notice that the charge transfer for the anionic clusters is larger than for the neutrals. A very interesting behavior similar to the neutral clusters, is that when 5 gold atoms are present, new bonds start to form between gold and oxygen, even if the charge is being provided by the rhodium. With the global minima structures (MA and DA) well identified we explored the minimum reaction paths between those two states. We have found again the following three possibilities:

- (I) The first case to discuss is $Au_4RhO_2^-$ where the multiplicity decreases as the oxygen molecule

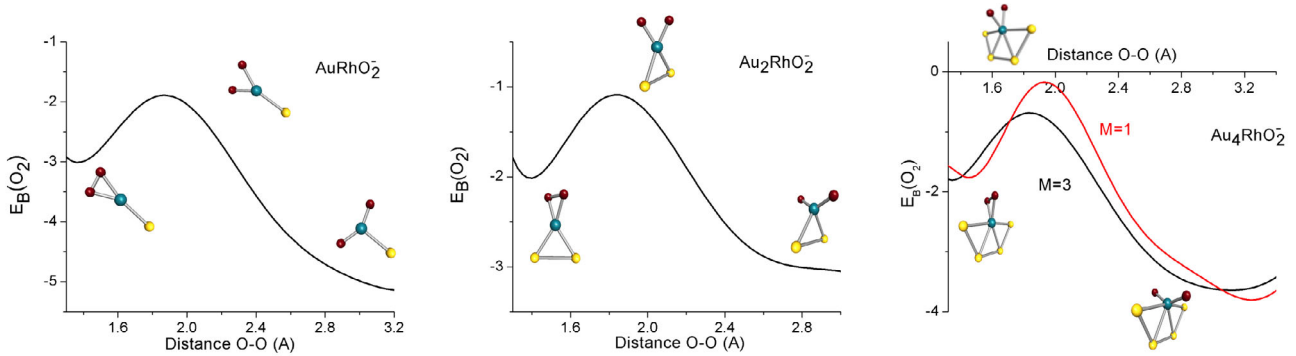


Fig. 5. Calculated reaction energy paths for the O_2 dissociation for $Au_nRhO_2^-$ ($n = 1, 2$ and 4) anionic clusters.

Table 3. Spin multiplicities, HOMO-LUMO gap's, oxygen binding energy, charge transfer from the cluster to the oxygen atoms and activation energies for both, MA and DA states for $Au_nRhO_2^-$, $n = 1-5$ anionic clusters.

| Cluster | 2S+1 | | GAP (H-L) (eV) | | $E_b(O_2)$ (eV) | | ΔQ (e^-) | E_{act} (eV) |
|---------------|------|----|-------------------|------|--------------------|------|-------------------------|-------------------|
| | MA | DA | MA | DA | MA | DA | | |
| | | | | | | | | |
| $AuRhO_2^-$ | 2 | 2 | 0.46 | 0.36 | 2.84 | 4.98 | 0.74 | 1.29 |
| $Au_2RhO_2^-$ | 3 | 3 | 0.51 | 0.50 | 1.84 | 3.45 | 0.60 | 0.95 |
| $Au_3RhO_2^-$ | 2 | 2 | 0.56 | 0.48 | 2.45 | 4.30 | 0.68 | 0.93 |
| $Au_4RhO_2^-$ | 3 | 1 | 0.56 | 0.55 | 1.84 | 3.79 | 0.68 | 1.82 |
| $Au_5RhO_2^-$ | 2 | 2 | 0.41 | 0.69 | 1.45 | 3.00 | 0.66 | 1.10 |

dissociates along the MEP. Notice how the different spin curves cross after the transition point, second notice that this cluster exhibits the biggest activation energy of all the anionic clusters (1.82 eV) see Figure 5c and Table 3.

- (II) Second, we have three clusters for which the multiplicity is always at the lowest possible along the dissociation trajectory ($AuRhO_2^-$, $Au_3RhO_2^-$ and $Au_5RhO_2^-$). Their corresponding activation energies are 1.29, 0.93 and 1.10 eV respectively and are reported in Table 3. A representative graph with the MEP for $AuRhO_2^-$ is shown in Figure 5a.
- (III) Finally $Au_2RhO_2^-$ with $M = 3$ maintains its unpaired electrons along the dissociation path, this system has one of the lowest activation energies (0.95 eV see Fig. 5b and Tab. 3). It is interesting that the smaller barriers belong to those systems whose spin configurations remain unaltered after the O_2 dissociation.

$Au_nRhO_2^+$

The cationic structures are significantly different to the bare Au_nRh^+ reported earlier in reference [37]. In the case of the molecularly bound state MA, we found non planar structures in general terms. Despite that, the rhodium atom remains the preferred O_2 binding site. On the other hand, the structures of $Au_nRhO_2^+$ for the dissociated

Table 4. Spin multiplicities, HOMO-LUMO gap's, oxygen binding energy, charge transfer from the cluster to the oxygen atoms and activation energies for both, MA and DA states for $Au_nRhO_2^+$, $n = 1-5$ cationic clusters.

| Cluster | 2S+1 | | GAP(H-L) (eV) | | $E_b(O_2)$ (eV) | | ΔQ (e^-) | E_{act} (eV) |
|---------------|------|----|------------------|------|--------------------|------|-------------------------|-------------------|
| | MA | DA | MA | DA | MA | DA | | |
| | | | | | | | | |
| $AuRhO_2^+$ | 2 | 2 | 0.33 | 0.51 | 0.97 | 2.48 | 0.58 | 2.42 |
| $Au_2RhO_2^+$ | 3 | 1 | 0.46 | 1.19 | 1.21 | 2.90 | 0.60 | 1.88 |
| $Au_3RhO_2^+$ | 2 | 2 | 0.50 | 0.84 | 1.47 | 2.48 | 0.62 | 1.74 |
| $Au_4RhO_2^+$ | 1 | 1 | 0.80 | 0.84 | 1.25 | 3.04 | 0.54 | 2.48 |
| $Au_5RhO_2^+$ | 2 | 2 | 0.56 | 0.25 | 1.14 | 1.70 | 0.52 | 1.18 |

states DA are again planar with the exemption of the oxygen atoms which are out of the plane (see Fig. 6). The cationic clusters binding energies are the smallest of all and are reported in Table 4. From the study of the MEP we can see that the activation energies range from 1.1 to 2.5 eV, and those are the highest of all. In this case the study of the reaction paths can only be separated in two possible scenarios:

- (I) First $Au_2RhO_2^+$ where the multiplicity decreases as the oxygen molecule dissociates along the MEP. Notice how the different spin curves also cross after the transition point, second notice that its barrier is larger than its corresponding neutral and anionic partner cluster (1.88 eV) see Figure 7a and Table 4.
- (II) Secondly, we have four clusters for which the multiplicity is always at the lowest possible configuration along the dissociation trajectory ($AuRhO_2^+$, $Au_3RhO_2^+$, $Au_4RhO_2^+$ and $Au_5RhO_2^+$). Their corresponding activation energies are 2.42, 1.74, 2.48 and 1.18 eV respectively and are reported in Table 4. Note that $Au_4RhO_2^+$ has the lowest possible multiplicity yet it poses the highest of all barriers. The MEP for $Au_3RhO_2^+$ is shown in Figure 7b.

Finally, we have calculated the total binding energy (E_b) according to the following expression:

$$E_b = E(Au_nRhO_2) - (nE(Au) - E(Rh) - 2E(O)).$$

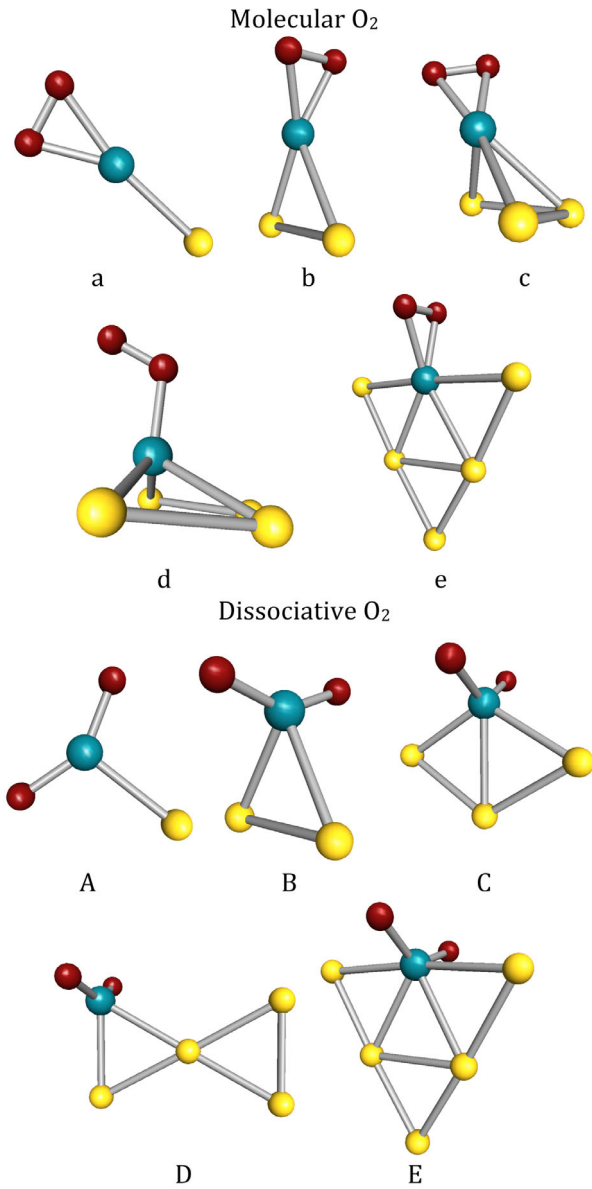


Fig. 6. Structures for atomic $Au_nRhO_2^+$ $n = 1-7$ cationic clusters with molecularly O_2 and dissociatively O_2 adsorbed onto their surfaces.

The binding energy of the DA systems is always higher than that of the MA ones as can be seen in columns 2 and 3 in Table 5. This result correlates well with our previous discussion of the $E_b(O_2)$ shown in Table 2 indicating that the contribution of the oxygen atoms is the main responsible in the total energy change. We have also calculated the electron affinities (EA) for Au_nRhO_2 complexes with $n = 1-5$ by means of the following expression:

$$EA = E(Au_nRhO_2) - E(Au_nRhO_2^-).$$

These values are reported in Table 5 for both, MA and DA states. The EA values vary typically in the range 2.5 to 4.2 eV. The larger values correspond to the DA mode complexes. This is concurrent with the higher stability finding for the DA states. The ionization potential (IP),

Table 5. Total binding energies, electron affinities and ionization potentials, at the molecular (MA) and the dissociative (DA) modes for Au_nRhO_2 $n = 1-5$.

| Cluster | E_b (eV) | | EA (eV) | | IP (eV) | |
|-------------|---------------|-------|------------|------|------------|------|
| | MA | DA | MA | DA | MA | DA |
| $AuRhO_2$ | 10.20 | 12.44 | 2.63 | 2.53 | 9.00 | 9.74 |
| Au_2RhO_2 | 12.50 | 14.01 | 2.53 | 2.63 | 8.10 | 7.92 |
| Au_3RhO_2 | 14.54 | 15.71 | 3.06 | 3.75 | 7.80 | 7.95 |
| Au_4RhO_2 | 16.60 | 17.31 | 2.88 | 4.12 | 7.63 | 7.63 |
| Au_5RhO_2 | 18.75 | 20.03 | 2.96 | 3.22 | 7.38 | 8.11 |

has also been calculated as follows:

$$IP = E(Au_nRhO_2^+) - E(Au_nRhO_2).$$

They are shown in Table 5. The IP values vary in the range 7.3 to 9.8 eV indicating good stability properties for these compounds.

We can summarize our results as follows: for the neutral, anionic and exclusively the DA cationic clusters the planar structures with the oxygen atoms out of plane prevail. The preferred interacting site for O_2 either as a molecule or dissociatively is at the rhodium atom. The DA structures of Au_5RhO_2 both, neutral and negatively charged are very peculiar because the oxygen excess interacts also with the gold atoms despite the charge excess offered by the Rh atom. In turn the dissociation mechanism of the O_2 molecule lures the oxygen atoms to a superoxo or peroxy-like states. The binding energy confirms the dissociatively adsorption state to be favored for all cases. We found an energy increase due to the O_2 molecule dissociation that is comparable to adding a gold atom to the mix i.e. $E_b(Au_nRhO_2)_{MA} \simeq E_b(Au_{n-1}RhO_2)_{DA}$. The lower barriers ($E_{act} \simeq 1.5$ eV) together with the relatively large oxygen-molecule oxygen binding energies ($E_b(O_2) \simeq 2.5$ eV) for the MA states, means that the anionic clusters are the best candidates for O_2 dissociation. Nevertheless, neutral clusters (Au_2RhO_2 , Au_3RhO_2 , Au_4RhO_2) have energy barriers which are lower than their corresponding O_2 binding energies. Finally, all cationic O_2 binding energies are too low compared with their activation barriers to be of interest. Examples between the different anion, neutral and cation (MA) \rightarrow (DA) reactions follow:

| Reaction | ΔE (eV) |
|--------------------------------------------------|-----------------|
| $Au_3RhO_2^-(MA) \rightarrow Au_3RhO_2^-(DA)$ | 0.93 |
| $Au_3RhO_2^-(MA) \rightarrow Au_3Rh^-(MA) + O_2$ | 2.45 |
| $Au_3RhO_2(MA) \rightarrow Au_3RhO_2(DA)$ | 1.16 |
| $Au_3RhO_2(MA) \rightarrow Au_3Rh(MA) + O_2$ | 1.57 |
| $Au_3RhO_2^+(MA) \rightarrow Au_3RhO_2^+(DA)$ | 1.74 |
| $Au_3RhO_2^+(MA) \rightarrow Au_3Rh^+(MA) + O_2$ | 1.47 |

The concentration of electronic charge at the rhodium site before the dissociation occurs, contributes to the decrease of the barrier, this charge is attracted by the oxygen atoms along the dissociation path. The characteristic even-odd stability behavior with the number of electrons earlier

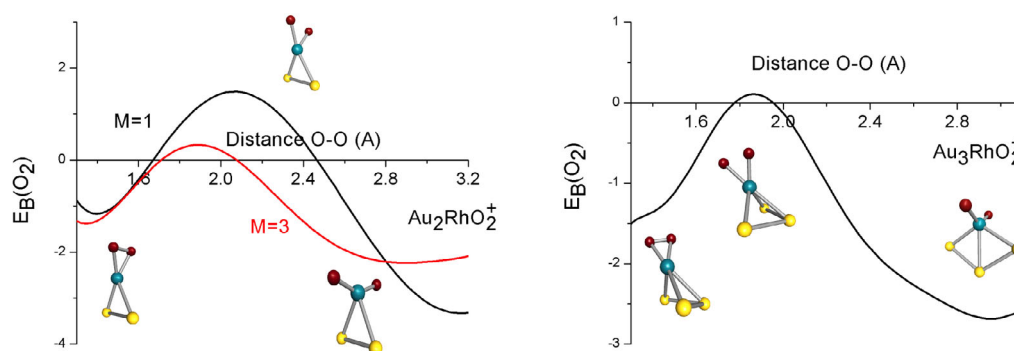


Fig. 7. Calculated reaction energy paths for the O_2 dissociation for $Au_nRhO_2^+$ ($n = 2$ and 3) cationic clusters.

observed in the pure gold case [14,16,20] is not present in the AuRh mix as far as this study concerns.

The adsorption process shifts the O-O stretching mode of the O_2 molecule from 1555 towards $\approx 1200\text{ cm}^{-1}$. During the dissociation process, the O-O stretching mode shifts even further (≈ 1200 towards $\approx 250\text{ cm}^{-1}$) and the symmetrical and antisymmetrical O-Rh-O stretching modes shift from ≈ 400 towards $\approx 850\text{ cm}^{-1}$ in the IR spectra. This reveals the O-O bond weakening, and the Rh-O bond strengthening. These shifts are clear fingerprints with the possibility to be easily observed in a future infrared experiment.

4 Conclusions

We have presented an extensive and systematic study on the interaction of the oxygen molecule with gas-phase gold-rhodium clusters in the size range of one to five gold atoms with one rhodium. We can conclude that the introduction of a dopant atom like rhodium provokes an enhancement of the reactivity properties of gold clusters towards oxygen. The energy barriers are the lowest for the anionic clusters and therefore are preferred for O_2 dissociation, with the difference but we do not observe a particular size behavior in their reactivity as it is seen in pure gold clusters [6,7,11,14,16,20]. The bonding mechanism involves charge transfer to the oxygen molecule with a concomitant activation of the O_2 bond to a peroxy or superoxy states. Infrared experiments should reveal dissociative from molecular states depending on the peak representative positions. Neutral and cationic Au_nRh clusters can also bind oxygen, although the interaction is much weaker and does not induce O-O dissociation that efficiently. We can conclude that the charge excess present at the rhodium atom is the driving force in the dissociation process. Finally, we found that when more gold atoms are present (5 atoms) new bonds start to form between gold and oxygen.

M.R.B. and F.B.Z. acknowledge support from PAPIIT IN100515, UNAM project, and from DGSCA UNAM. The calculations were performed at the supercomputer Miztli at the supercomputer center in UNAM, and to the IIM (Instituto

de Investigaciones en Materiales) for the use of its facilities. F.B.Z. acknowledges support from CONACYT (financial support No. 379750).

References

1. M. Haruta, *Catal. Today* **36**, 153 (1997)
2. M. Haruta, N. Yamada, T. Kobayashi, S. Iijima, *J. Catal.* **115**, 301 (1989)
3. M. Haruta, S. Tsubota, S. Kobayashi, H. Kageyama, M.J. Genet, B.J. Delmon, *J. Catal.* **144**, 175 (1993)
4. M. Daté, M. Haruta, *J. Catal.* **201**, 221 (2001)
5. V. Bonačić-Koutecký, J. Burda, R. Mitrić, M. Ge, G. Zampella, P. Fantucci *J. Chem. Phys.* **117**, 3120 (2002)
6. C. Bürgel, N.M. Reilly, G.E. Johnson, R. Mitrić, M.L. Kimble, A.W. Castleman Jr., *J. Am. Chem. Soc.* **130**, 1694 (2008)
7. G.E. Johnson, R. Mitrić, V. Bonačić-Koutecký, A.W. Castleman Jr., *Chem. Phys. Lett.* **479**, 1 (2009)
8. B. Yoon, H. Häkkinen, U. Landman, A.S. Wörz, J.M. Antonietti, S. Abbet, K. Judai, U. Heiz, *Science* **307**, 403 (2005)
9. A. Fielicke, P. Gruene, G. Meijer, D.M. Rayner, *Surface Science* **603**, 1427 (2009)
10. P. Gruene, B. Butschke, H.T. Lyon, D.M. Rayner, A. Fielicke, *Z. Phys. Chem.* **480**, 337 (2014)
11. M.L. Kimble, A.W. Castleman Jr., C. Bürgel, V. Bonačić-Koutecký, *Int. J. Mass Spectrom.* **254**, 163 (2006)
12. W.T. Wallace, R.B. Wyrwas, R.L. Whetten, R. Mitrić, V. Bonačić-Koutecký, *J. Am. Chem. Soc.* **125**, 8408 (2003)
13. W.T. Wallace, R.L. Whetten, *J. Am. Chem. Soc.* **124**, 7499 (2002)
14. H. Häkkinen, U. Landman, *Phys. Rev. B* **62**, R2287 (2000)
15. A.P. Woodham, A. Fielicke, *Angew. Chem. Int. Ed.* **53**, 6554 (2014)
16. L.M. Molina, B. Hammer, *J. Chem. Phys.* **123**, 161104 (2005)
17. L.M. Molina, M.D. Rasmussen, B. Hammer, *J. Chem. Phys.* **120**, 7673 (2004)
18. X. Ding, Z. Li, J. Yang, J.G. Hou, Q. Zhu, *J. Chem. Phys.* **120**, 9594 (2004)
19. Q. Sun, P. Jena, *J. Chem. Phys.* **120**, 6510 (2014)
20. L. Xiao, B. Tollberg, X. Hu, L. Wang, *J. Chem. Phys.* **124**, 114309 (2006)
21. J. Hagen, L.D. Socaciu, M. Eljazyfer, U. Heiz, T.M. Bernhardt, L. Wöste, *Phys. Chem. Chem. Phys.* **4**, 1707 (2002)

22. L.D. Socaciu, J. Hagen, T.M. Bernhardt, L. Wöste, U. Heiz, H. Häkkinen, U. Landman, *J. Am. Chem. Soc.* **125**, 10437 (2003)
23. S.A. Varganov, R.M. Olson, M.S. Gordon, H. Metiu, *J. Chem. Phys.* **119**, 2531 (2003)
24. L.B. Vilhelmsen, B. Hammer, *Phys. Rev. Lett.* **108**, 126101 (2012)
25. R. Ferrando, J. Jellinek, R.L. Johnston, *Chem. Rev.* **108**, 845 (2008)
26. R.L. Chantry, I. Atanasov, S.L. Horswell, Z.Y. Li, R.L. Johnston, *Gold Clusters, Colloids and Nanoparticles II* (Springer, Switzerland, 2014), pp. 67–90
27. R.L. Johnston, R. Ferrando, *Faraday Discuss.* **138**, 1 (2008)
28. *Nanoalloys: From Fundamentals to Emergent Applications*, edited by F. Calvo (2013), Vol. 1
29. S. Moussa, V. Abdelsayed, M.S. El Shall, *Nanoalloys* **1**, 1 (2013)
30. P. Ghosh, R. Pushpa, S. de Gironcoli, S. Narasimhan., *J. Chem. Phys.* **128**, 194708 (2008)
31. S.M. Hamilton, W.S. Hopkins, D.J. Harding, T.R. Walsh, P. Gruene, M. Haertelt, A. Fielicke, G. Meijer, S.R. Mackenzie, *J. Am. Chem. Soc.* **132**, 1448 (2010)
32. X. Li, A. Grubisic, S.T. Stokes, J. Cordes, G.F. Gantefoer, K.H. Bowen, B. Kiran, M. Willis, P. Jena, R. Burgert, H. Schnoekel, *Science* **315**, 356 (2007)
33. M.L. Anderson, M.S. Ford, P.J. Derrick, T. Drewello, D.P. Woodruff, S.R. Mackenzie, *J. Phys Chem.* **110**, 10992 (2006)
34. M.S. Ford, M.L. Andreson, M.P. Barrow, D.P. Woodruff, T. Drwello, P.J. Derrick, S.T. Mackenzie, *Phys. Chem. Chem. Phys.* **7**, 975 (2005)
35. S.L. Romo-Ávila, R.A. Guirado-lópez, *J. Phys. Chem. A* **116**, 1059 (2012)
36. M.R. Beltrán, F. Buendía, V. Chauhan, P. Sen, H. Wang, Y.J. Ko, L. Bowen, *Eur. J. Phys. D* **67**, 63 (2013)
37. F. Buendía, M.R. Beltrán, X. Zhang, G. Liu, A. Buytendyk, K. Bowen, *J. Phys. Chem. Chem. Phys.* **17**, 28219 (2015)
38. F. Weigend, R. Ahlrichs, *Phys. Chem. Chem. Phys.* **7**, 3297 (2005)
39. J.P. Perdew, K. Burke, M. Ernzerhof, *Phys. Rev. Lett.* **77**, 3865 (1996)
40. M.P. Johansson, A. Lechtken, D. Schoos, M.M. Kappes, F. Furche, *Phys. Rev. A* **77**, 053202 (2008)
41. M. Mantina, R. Valero, D.G. Truhlar, *J. Chem. Phys.* **131**, 064706 (2009)
42. R. Ahlrichs, M. Bar, M. Haser, H. Horn, C. Kolmel, *Chem. Phys. Lett.* **162**, 165 (1989)
43. Yang Ji-Xian, Wei Cheng-Fuand, Guo Jian-Jun, *Physica B* **405**, 4892 (2010)
44. K.A. Gingerich, D.L. Cocke, *J. Chem. Soc. Chem. Commun.* **1**, 536 (1972)
45. K.P. Huber, G. Herzberg, in: *Molecular Spectra and Molecular structure IV. Constants of Diatomic Molecules* (Van Nostrand Reinhold Company, New York, 1979), p. 198
46. V.I. Vedeneyev, L.V. Gurvich, V.N. Kondratyev, V.A. Medvedev, Ye.L. Frankevich, *Bond Energies, Ionization Potentials and Electron Affinities* (St. Martin's Press, New York, 1962)
47. H. Jonsson, G. Millsa, K.W. Jacobsen, *Nudged Elastic Band Method for Finding Minimum Energy Paths of Transitions* (World Scientific, 1998), p. 385